4-Anilinoquinazoline-based benzenesulfonamides as nanomolar inhibitors of carbonic anhydrase isoforms I, II, IX, and XII: design, synthesis, *in-vitro*, and *in-silico* biological studies

Hossam Nada, Ahmed Elkamhawy, Magda H. Abdellattif, Andrea Angeli, Chang Hoon Lee, Claudiu T. Supuran & Kyeong Lee

View supplementary material

Published online: 30 Mar 2022.

Submit your article to this journal

Article views: 2018

View related articles

View Crossmark data

Citing articles: 14 View citing articles

Taylor & Francis
Taylor & Francis Group

RESEARCH PAPER

OPEN ACCESS | Check for updates

4-Anilinoquinazoline-based benzenesulfonamides as nanomolar inhibitors of carbonic anhydrase isoforms I, II, IX, and XII: design, synthesis, *in-vitro*, and *in-silico* biological studies

Hossam Nada[a]* (ID), Ahmed Elkamhawy[a,b]* (ID), Magda H. Abdellattif[c] (ID), Andrea Angeli[d] (ID), Chang Hoon Lee[a], Claudiu T. Supuran[d] (ID) and Kyeong Lee[a]

[a]BK21 FOUR Team and Integrated Research Institute for Drug Development, College of Pharmacy, Dongguk University-Seoul, Goyang, Republic of Korea; [b]Department of Pharmaceutical Organic Chemistry, Faculty of Pharmacy, Mansoura University, Mansoura, Egypt; [c]Department of Chemistry, College of Science, Taif University, Taif, Saudi Arabia; [d]NEUROFARBA Department, Sezione di Scienze Farmaceutiche, University of Florence, Sesto Fiorentino, Florence, Italy

ABSTRACT
Human carbonic anhydrase inhibitors (hCAIs) are a key therapeutic class with a multitude of novel applications such as anticonvulsants, topically acting antiglaucoma, and anticancer drugs. Herein, a new series of 4-anilinoquinazoline-based benzenesulfonamides were designed, synthesised, and biologically assessed as potential hCAIs. The target compounds are based on the well-tolerated kinase scaffold (4-anilinoquinazoline). Compounds **3a** (89.4 nM), **4e** (91.2 nM), and **4f** (60.9 nM) exhibited 2.8, 2.7, and 4 folds higher potency against hCA I when compared to the standard (AAZ, **V**), respectively. A single digit nanomolar activity was elicited by compounds **3a** (8.7 nM), **4a** (2.4 nM), and **4e** (4.6 nM) with 1.4, 5, and 2.6 folds of potency compared to AAZ (12.1 nM) against isoform hCA II, respectively. Structure-activity relationship (SAR) and molecular docking studies validated our design approach that revealed highly potent hCAIs.

1. Introduction

Carbonic anhydrases (CAs) are metalloenzymes responsible for converting CO_2 to bicarbonate and proton in living organisms[1]. Human CAs of the α-class (α-CA) can be additionally grouped into sixteen isoforms that vary in cellular localisation, oligomeric structure, allocation in organs and tissues, kinetic properties, expression levels, and molecular characteristics[2]. Each isoform exhibits a specific subcellular localisation; CA I, II, III, VII, and XIII are cytosolic, CA IV, IX, XII, XIV, and XV are membrane-associated, while CA VA and VB are mitochondrial, and CA VI is secreted[3–5]. CAs are involved in a number of physiological activities such as breathing, pH regulation, bone resorption, ion transport, and gastric fluid secretion[6]. Consequently, CA inhibitors have become a leading therapeutic class in recent decades. Anticancer agents, anticonvulsants and topically acting antiglaucoma are some of the novel applications of CA inhibitors that have been reported[2,7]. Due to its expression in the endothelium of neovessels in melanoma, renal, lung, and oesophageal cancers, CA II is the most physiologically relevant isoform which was linked with various tumours including melanoma, oesophageal, renal, and lung cancers[8]. Inhibition of CA II also decreases angiogenesis *via* inhibition of vascular endothelial growth factor receptor (VEGFR) signaling[9]. The most common approach in designing CA inhibitors has been through the modulation of the ring directly bound to the zinc binding group (ZBG) or by attaching different "tails" to the aromatic ring as demonstrated by compounds **I–III** (Figure 1)[10–13].

Sulphonamides are a well-known ZBG moieties possessing effective carbonic anhydrase inhibitory activities, compounds **I–III** (Figure 1)[12]. Aromatic sulphonamides are reported to be strong and specific inhibitors of CA isoforms and deemed to be promising leads for further modifications and development of more potent inhibitors[13]. However, the lack of selectivity in blocking distinct isoforms is a key downside of CAIs, which is caused by structural similarity and identical subcellular location of these isoforms, resulting in adverse side effects[14]. Among the studied sulphonamides, the primary sulphonamide is one of the most effective ZBG for designing carbonic anhydrases inhibitors. This is owing to structural features that make them optimal for binding to the Zn^{2+} ion in the active site cavity and surrounding residues[15–17]. The negatively charged nitrogen of SO_2NH^- binds to the positively charged metal ion substituting the physiological zinc-bound nucleophile, where the proton found on the coordinated nitrogen atom acting as an acceptor via being at H-bond distance to Thr199 OG1 atom[16]. Several sulphonamide-based carbonic anhydrase inhibitors are currently in clinical trial targeting various diseases, such as SLC-0111 (**IV**, Figure 2) which is currently in phase I clinical trials as for patients with advanced tumours[18]. Acetazolamide (**V**, Figure 2) and Methazolamide (**VI**, Figure 2) are two examples of sulphonamide-based drugs which are currently
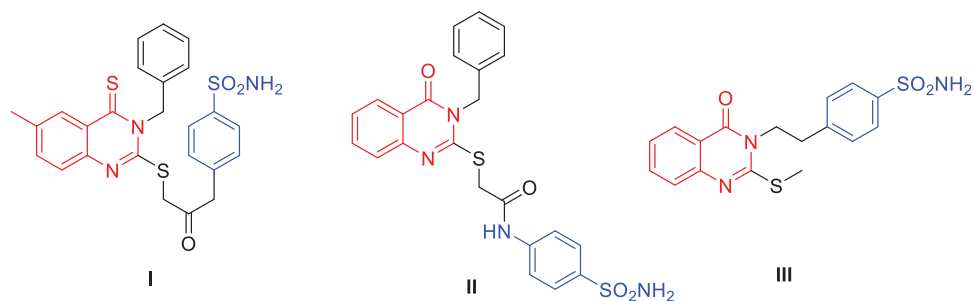
Figure 1. Chemical structures of potent quinazoline-based analogues as carbonic anhydrase inhibitors possessing primary sulphonamide (ZBG) moiety.
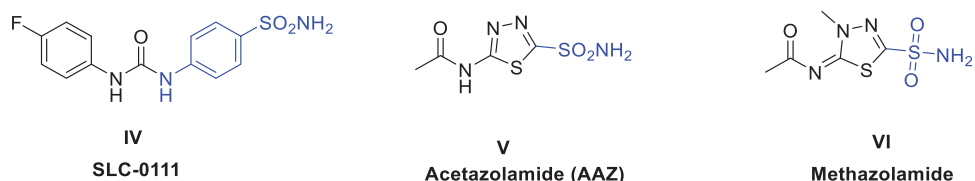

Figure 2. Chemical structure of some of the small molecule inhibitors currently in clinical trials.
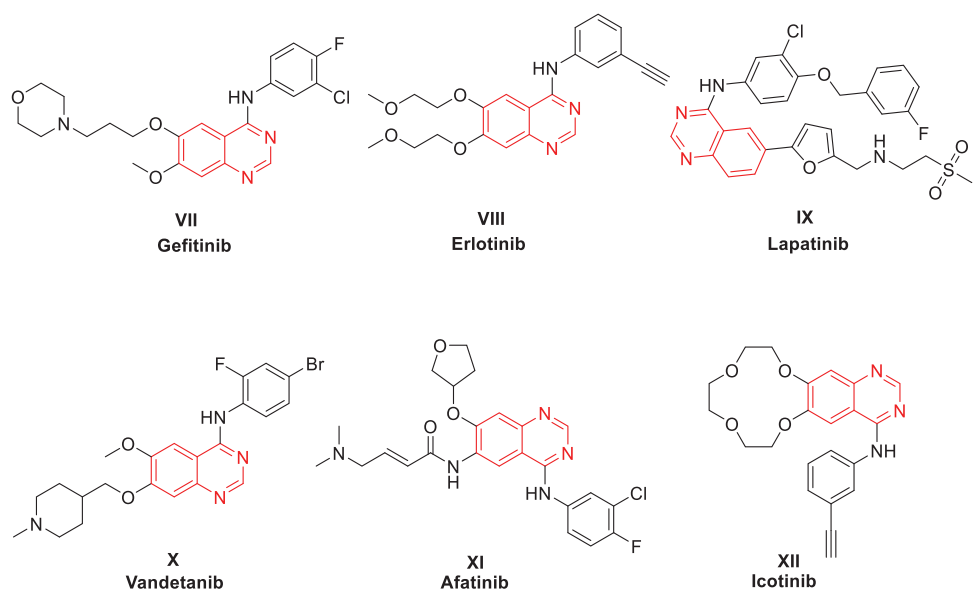

Figure 3. FDA approved 4-Anilinoquinazolines tyrosine kinase inhibitors.

undergoing phase IV clinical trials as carbonic anhydrase I inhibitors[19,20].

4-Anilinoquinazolines have been frequently explored as anticancer agents due to their reported inhibitory activity on various receptor tyrosine kinases, such as VEGFR-2 (Vascular endothelial growth factor receptor 2), EGFR (epidermal growth factor receptor), or receptor tyrosine-protein kinase erbB-2 (HER2[21,22]. As illustrated in Figure 3, this heterocyclic class includes several approved drugs such as Gefitinib (Iressa®, **VII**), Erlotinib (Tarceva®, **VIII**), Lapatinib (Tykreb®, **IX**), Vandetanib (Caprelsa®, **X**), Afatinib (Gilotrif®, **XI**), and Icotinib (**XII**). Gefitinib (EGFR inhibitor) was approved by the FDA on May 2003 as a monotherapy to treat patients suffering from locally advanced or metastatic non-small cell lung cancer (NSCLC) following the failure of both platinum-based and docetaxel chemotherapies[23]. One year later, Erlotinib (EGFR inhibitor) was approved for treating NSCLC and in conjunction with gemcitabine for treatment of locally advanced, unrespectable, or metastatic pancreatic cancer[24]. In 2010, Lapatinib was approved for breast cancer treatment[25]. Lapatinib acts via

inhibiting both HER2 and EGFR pathways and is utilised in combination therapies for HER2-positive breast cancer[26]. A year later, Vandetanib (a multi-kinase inhibitor) was approved as a treatment of metastatic medullary thyroid cancer[27]. Vandetanib exerts action through the inhibition of VEGFR, EGFR, and the RET-tyrosine kinase. Afatinib (EGFR/HER2 dual inhibitor) and Icotinib (EGFR inhibitor) were also approved for treatment of NSCLC[28,29]. These discoveries validate that 4-anilinoquinazoline is a privileged scaffold for developing anticancer drugs. Furthermore, the quinazoline ring was proved to be well-tolerated in the biological systems in terms of safety and potency[30,31].

In the recent decade, some trials to develop quinazoline-based sulphonamides as CA inhibitors have been conducted. In 2014, a novel series of 2-substituted-mercapto-3-substituted-4(3H)-quinazolinones (**I**, Figure 1) was reported as α-carbonic anhydrases inhibitors from *Vibrio cholerae*[32]. Despite the high potency of these derivatives against *Vibrio cholerae*, they exhibited low inhibitory activity for the hCA I isoform (K_i range: 0.793–4.55 μM) and modest activity against the hCA II isoform (K_i range:
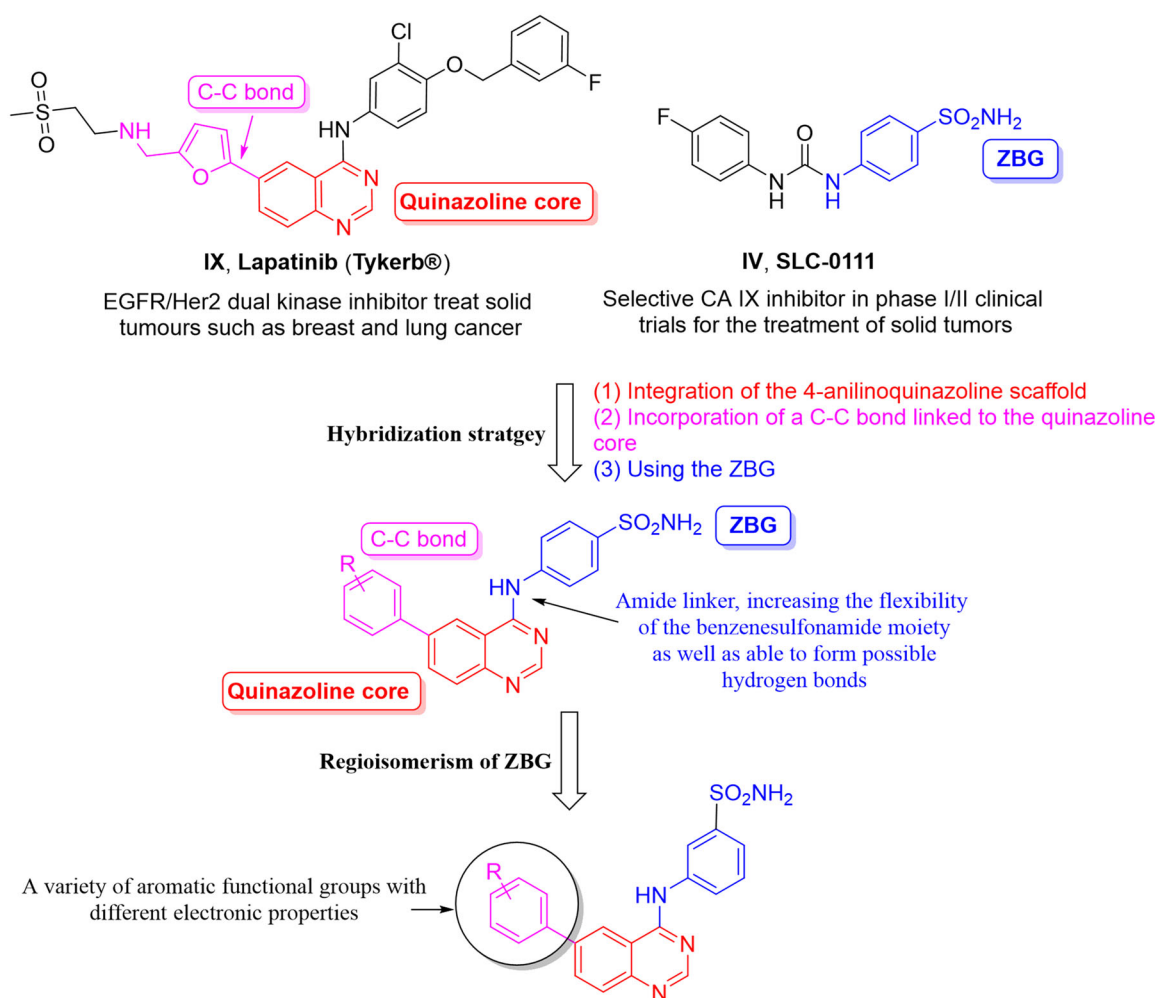
Figure 4. Design of the target hCAIs.

65.3 nM–0.114 μM). In the same year, another series of 4-oxoquinazoline containing a benzenesulfonamide moiety (**II**, Figure 1) was reported as a novel CA inhibitor against the protozoan enzyme of *Trypanosoma cruzi*[33]. The Oxoquinazoline (**II**) demonstrated moderate inhibition when tested against hCA I (K_i range: 86.5 nM–5.43 μM) and a higher potency over hCA II isoforms. However, they have not been tested against the cancer-related hCA IX and XII isoforms.

Resuming the efforts of developing effective quinazoline-based hCA inhibitors, a new series of novel 4-anilinoquinazoline-based sulphonamides were designed and synthesised (Figure 4). The effect of the aromatic substitutions at positions 4, 6 and 7 of the quinazoline core, as hCA inhibitor, is largely undiscovered. Therefore, a structural hybridisation strategy (Figure 4) was utilised through incorporating the benzenesulfonamide moiety of SLC-0111 (**IV**) at position 4 of the quinazoline ring. We have also incorporated various aromatic substitutions at positions 6 and 7 of the quinazoline scaffold including **3a**, **4a**–**f**, **4h** and **4j**. These compounds tested the effects of different hydrophilic substitutions as in compounds **4b**, **4d**, **4h** and **4j** as well as the effect of hydrophobic substitutions as in compounds **3a**, **4a**, **4c**, **4e** and **4f**. In addition to the difference in hydrophilicity and size of the substitutions, the substitutions chosen also possessed different electronic properties to establish key interactions within the roomy hCA binding sites. Thereafter, a regioisomerism strategy was

applied to afford the *meta*-sulfamoyl ZBG derivatives, regioisomers **3b**, **4i** and **4k**–**l**. The hybridisation strategy incorporated the C-C bond from Lapatinib (**IX**) to attach the aromatic substitutions to increase the rigidity of the tail region in a similar manner to the Lapatinib. On the other hand, a flexible amino linker was used to link the quinazoline moiety with the sulphonamide moiety to increase the possibility of hydrogen bond formation as well as grant suitable flexibility to the sulphonamide region to bind easily with Zn metal of the active site.

The target compounds designed herein were synthesised, characterised, and assessed for their hCA inhibitory activity against its four isoforms I, II, IX and XII. Then, the structure-activity relationship (SAR) was discussed. A molecular docking study was carried out to increase the understanding of the hCA inhibitory action of the target compounds.

2. Materials and methods

2.1. Chemistry

2.1.1. General
In the conducted experiments all acquired solvents and reagents were applied without additional purification. Varian 400 MHz spectrometer (Varian Medical Systems, Inc., Palo Alto, CA, USA) was utilised to calculate the ^{1}H NMR spectra with chemical shifts being

measured in parts per million (ppm) and coupling constants in Hz. The high-resolution electrospray ionisation mass spectrometry (HR-ESIMS) data were assessed utilising a JMS–700 mass spectrometer (Jeol, Japan) or by HR-ESIMS data obtained via a G2 QTOF mass spectrometer. Reaction monitoring was carried out using TLC on 0.25 mm silica plates (E. Merck; silica gel 60 F_{254}). Reverse-phase high performance liquid chromatography (RP-HPLC) was employed to determine the purity of the products, with the UV detector of the HPLC being set at 254 nm. The mobile phases employed were: (A) H_2O containing 0.05% TFA and (B) CH_3CN. The purity of the final compound was determined using a gradient of 75% B or 100% B in 30 min. The melting points were measured using a Fisherbrand digital melting point apparatus. Compounds **2a–b** and **3a–d** were synthesised as reported earlier[34]. The final target compounds were synthesised following the reported procedure of Suzuki cross-coupling reaction[34].

4-((6-phenylquinazolin-4-yl)amino)benzenesulfonamide (4a). Off-white solid, Yield: 35%, mp: 310–312 °C, HPLC purity: 15 min, 98.56%, ^{1}H NMR (400 MHz, DMSO-d_6) δ 10.14 (s, 1H), 8.85 (s, 1H), 8.66 (s, 1H), 8.21 (d, $J = 12.0$ Hz, 1H), 8.08 (d, $J = 8.0$ Hz, 2H), 7.91–7.80 (m, 5H), 7.55 (t, $J = 8.0$ Hz, 2H), 7.43 (t, $J = 4.0$ Hz, 1H), 7.29 (s, 2H). ^{13}C NMR (100 MHz, DMSO-d_6) δ 158.09, 154.66, 149.76, 149.56, 142.71, 139.53, 138.85, 132.58, 129.50, 128.97, 128.47, 127.66, 126.75, 122.08, 120.95, 115.87. HRMS (ESI) *m/z* calculated for $C_{20}H_{17}N_4O_2S$ [M + H]$^+$: 377.1067, found: 377.1072.

4-((6–(4-formylphenyl)quinazolin-4-yl)amino)benzenesulfonamide (4b). Off-white solid, Yield: 46%, mp: 265–267 °C, HPLC purity: 17 min, 94.26%, ^{1}H NMR (400 MHz, DMSO-d_6) δ 10.20 (s, 1H), 10.08 (s, 1H), 8.97 (s, 1H), 8.68 (s, 1H), 8.30 (d, $J = 8.0$ Hz, 1H), 8.13 (d, $J = 8.0$ Hz, 2H), 8.10–8.04 (m, 4H), 7.92 (d, $J = 8.0$ Hz, 1H), 7.84 (d, $J = 8.0$ Hz, 2H), 7.28 (s, 2H). ^{13}C NMR (100 MHz, DMSO-d_6) δ 193.22, 158.23, 155.18, 150.20, 145.11, 142.58, 139.11, 137.24, 135.85, 132.56, 130.65, 129.19, 128.28, 126.78, 122.21, 115.88. HRMS (ESI) *m/z* calculated for $C_{21}H_{17}N_4O_3S$ [M + H]$^+$: 405.1016, found: 405.1021.

4-((6–(4-fluorophenyl)quinazolin-4-yl)amino)benzenesulfonamide (4c). White solid, Yield: 26%, mp: 325–327 °C, HPLC purity: 17 min, 95.19%, ^{1}H NMR (400 MHz, DMSO-d_6) δ 10.13 (s, 1H), 8.82 (s, 1H), 8.66 (s, 1H), 8.19 (d, $J = 8.0$ Hz, 1H), 8.07 (d, $J = 8.0$ Hz, 2H), 7.95–7.79 (m, 5H), 7.39 (t, $J = 12.0$ Hz, 2H), 7.28 (s, 2H). ^{13}C NMR (100 MHz, DMSO-d_6) δ 163.87, 161.44, 158.07, 154.70, 149.55, 142.68, 138.98, 137.73, 136.04, 132.48, 129.74, 126.76, 122.08, 120.89, 116.46, 115.84. HRMS (ESI) *m/z* calculated for $C_{20}H_{16}FN_4O_2S$ [M + H]$^+$: 395.0973, found: 395.0977.

4-((6–(3-nitrophenyl)quinazolin-4-yl)amino)benzenesulfonamide (4d). Off-white solid, Yield: 47%, mp: 335–337 °C, HPLC purity: 17 min, 95.08%, ^{1}H NMR (400 MHz, DMSO-d_6) δ 10.21 (s, 1H), 8.96 (s, 1H), 8.68 (s, 2H), 8.34–8.30 (m, 8.7 Hz, 3H), 8.07 (d, $J = 8.0$ Hz, 2H), 7.93 (d, $J = 8.0$ Hz, 1H), 7.87–7.81 (m, 3H), 7.29 (s, 2H). HRMS (ESI) *m/z* calculated for $C_{20}H_{16}N_5O_4S$ [M + H]$^+$: 422.0918, found: 422.0909.

4-((6–(4-methoxyphenyl)quinazolin-4-yl)amino)benzenesulfonamide (4e). Off-white solid, Yield: 40%, mp: 327–329 °C, HPLC purity: 17 min, 96.57%, ^{1}H NMR (400 MHz, DMSO-d_6) δ 10.10 (s, 1H), 8.78 (s, 1H), 8.64 (s, 1H), 8.17 (d, $J = 8.0$ Hz, 1H), 8.07 (d, $J = 12.0$ Hz, 2H), 7.87–7.80 (m, 5H), 7.27 (s, 2H), 7.10 (d, $J = 8.0$ Hz, 2H), 3.82 (s, 3H). ^{13}C NMR (100 MHz, DMSO-d_6) δ 159.81, 157.97, 154.33,

149.23, 142.77, 138.90, 138.51, 132.25, 131.81, 128.81, 126.74, 122.04, 119.89, 115.91, 114.94, 55.74. HRMS (ESI) *m/z* calculated for $C_{21}H_{19}N_4O_3S$ [M + H]$^+$: 407.1172, found: 407.1171.

4-((6-(thiophen-3-yl)quinazolin-4-yl)amino)benzenesulfonamide (4f). Off-white solid, Yield: 40%, mp: 259–262 °C, HPLC purity: 15 min, 97.18%, ^{1}H NMR (400 MHz, DMSO-d_6) δ 10.04 (s, 1H), 8.84 (s, 1H), 8.63 (s, 1H), 8.27 (d, $J = 8.0$ Hz, 1H), 8.07 (d, $J = 8.0$ Hz, 3H), 7.87–7.72 (m, 5H), 7.28 (s, 2H). ^{13}C NMR (100 MHz, DMSO-d_6) δ 157.96, 154.44, 149.43, 142.68, 140.98, 138.97, 133.82, 132.13, 128.92, 128.01, 126.86, 122.73, 122.08, 119.76, 115.88. HRMS (ESI) *m/z* calculated for $C_{18}H_{15}N_4O_2S_2$ [M + H]$^+$: 383.0631, found: 383.0626.

3-((6–(4-fluorophenyl)quinazolin-4-yl)amino)benzenesulfonamide (4g). White solid, Yield: 54%, mp: 277–279 °C, HPLC purity: 16 min, 100%, ^{1}H NMR (400 MHz, DMSO-d_6) δ 10.16 (s, 1H), 8.86 (s, 1H), 8.65 (s, 1H), 8.37 (s, 1H), 8.24–8.17 (m, 2H), 7.99–7.86 (m, 3H), 7.65–7.57 (m, 2H), 7.42 (t, $J = 8.0$ Hz, 4H). ^{13}C NMR (100 MHz, DMSO-d_6) δ 163.86, 161.42, 158.16, 154.75, 149.49, 144.89, 140.03, 137.67, 136.06, 132.38, 129.76, 128.96, 121.10, 120.87, 119.49, 116.46, 116.24, 115.75. HRMS (ESI) *m/z* calculated for $C_{20}H_{16}FN_4O_2S$ [M + H]$^+$: 395.0973, found: 395.0971.

4-((6–(4-morpholinophenyl)quinazolin-4-yl)amino)benzenesulfonamide (4h). Off- white solid, Yield: 42%, mp: 227–229 °C, HPLC purity: 15 min, 95.27%, ^{1}H NMR (400 MHz, DMSO-d_6) δ 10.12 (s, 1H), 8.78 (s, 1H), 8.65 (s, 1H), 8.20 (d, $J = 12.0$ Hz, 1H), 8.11 (d, $J = 12.0$ Hz, 2H), 7.87–7.81 (m, 5H), 7.30 (s, 2H), 7.12 (d, $J = 8.0$ Hz, 2H), 3.79–3.77 (m, 4H), 3.23–3.21 (s, 4H). ^{13}C NMR (100 MHz, DMSO-d_6) δ 157.90, 154.12, 151.50, 149.07, 142.81, 138.86, 131.96, 129.71, 128.81, 128.16, 126.73, 122.03, 119.20, 115.79, 66.46, 48.48. HRMS (ESI) *m/z* calculated for $C_{24}H_{24}N_5O_3S$ [M + H]$^+$: 462.1594, found: 462.1592.

3-((6–(5-formylfuran-2-yl)quinazolin-4-yl)amino)benzenesulfonamide (4i). Off-white solid, Yield: 28%, mp: 260–262 °C, HPLC purity: 13 min, 95.09%, ^{1}H NMR (400 MHz, DMSO-d_6) δ 10.38 (s, 1H), 9.69 (s, 1H), 9.08 (s, 1H), 8.67 (s, 1H), 8.35 (s, 2H), 8.19 (s, 1H), 7.92 (d, $J = 12.0$ Hz, 1H), 7.77 (d, $J = 4.0$ Hz, 1H), 7.62 (s, 2H), 7.48–7.39 (m, 3H). HRMS (ESI) *m/z* calculated for $C_{19}H_{15}N_4O_4S$ [M + H]$^+$: 395.0809, found: 395.0804.

4-((7–(3-hydroxyphenyl)quinazolin-4-yl)amino)benzenesulfonamide (4j). Yellow solid, Yield: 22%, mp: 312–314 °C, HPLC purity: 13 min, 96.82%, ^{1}H NMR (400 MHz, DMSO-d_6) δ 10.10 (s, 1H), 9.67 (s, 1H), 8.72–8.64 (m, 2H), 8.14 (d, $J = 12.0$ Hz, 2H), 7.97 (d, $J = 12.0$ Hz, 2H), 7.85 (d, $J = 8.0$ Hz, 2H), 7.37–7.20 (m, 5H), 6.88 (d, $J = 8.0$ Hz, 1H). ^{13}C NMR (100 MHz, DMSO-d_6) δ 158.44, 157.87, 155.14, 152.27, 145.32, 145.12, 142.84, 140.48, 140.28, 138.75, 136.71, 136.5, 130.55, 121.68, 118.48, 114.73, 114.22. HRMS (ESI) *m/z* calculated for $C_{20}H_{17}N_4O_3S$ [M + H]$^+$: 393.1016, found: 393.1009.

3-((7–(3-hydroxyphenyl)quinazolin-4-yl)amino)benzenesulfonamide (4k). Off-white solid, Yield: 18%, mp: 302–304 °C, HPLC purity: 15 min, 99.32%, ^{1}H NMR (400 MHz, DMSO-d_6) δ 10.08 (s, 1H), 9.68 (s, 1H), 8.69–8.66 (m, 2H), 8.43 (s, 1H), 8.20 (s, 1H), 7.96 (d, $J = 8.0$ Hz, 2H), 7.62–7.58 (m, 2H), 7.44–7.28 (m, 4H), 7.22 (s, 1H), 6.87 (d, $J = 8.0$ Hz, 1H). HRMS (ESI) *m/z* calculated for $C_{20}H_{17}N_4O_3S$ [M + H]$^+$: 393.1016, found: 393.1010.

3-((6-phenylquinazolin-4-yl)amino)benzenesulfonamide (4l). Off-white powder, Yield: 24%, mp: 327–329 °C, HPLC purity: 14 min, 99.81%, ^{1}H NMR (400 MHz, DMSO-d_6) δ 10.16 (s, 1H), 8.89 (s, 1H), 8.65 (s, 1H), 8.37 (s, 1H), 8.24–8.21 (m, 2H), 7.91 (d, $J = 8.0$ Hz, 3H), 7.60–7.57 (m, 4H), 7.50–7.40 (m, 3H). HRMS (ESI) m/z calculated for $C_{20}H_{17}N_4O_2S$ $[M + H]^+$: 377.1067, found: 377.1066.

2.2. Carbonic anhydrase inhibition study

The activity of the CA-catalyzed CO_2 hydration reaction was evaluated employing an applied photophysics stopped-flow instrument. The indicator, Phenol red (at a concentration of 0.2 mM) was added to the CA-catalyzed CO_2 hydration reaction after a period of 10–100 s. Phenol red functioned at an absorbance maximum of 557 nm, with 20 mM Hepes (pH 7.4) and 10 mM $NaClO_4$ (to retain constant ionic strength)[35]. A CO_2 concentration ranging between 1.7 and 17 mM was employed to evaluate the kinetic parameters and inhibition constants[33]. A minimum of six traces of the starting 5–10% of the reaction were analysed to measure the initial velocity for each inhibitor. In a similar manner, the uncatalyzed rates were evaluated and subtracted from the overall calculated rates[36]. Stock inhibitor solutions (10 mM) were prepared in distilled–deionized water, and dilutions up to 0.01 nM were prepared with distilled–deionized water after that. Preincubation of the inhibitor enzyme solutions at room temperature to enable the formation of the E-I complex was carried out for 15 min before starting the experiment. The inhibition constants were determined employing PRISM 3, while the kinetic parameters for the uninhibited enzymes were calculated using Lineweaver-Burk plots that comprise the mean of at least three separate measurements with errors ranging to ±5–10% of the stated values[37,38].

2.3. Molecular docking study

The crystal structures of carbonic anhydrase isoforms hCA I (PDB code: 6Y00, resolution 1.37 Å)[39], hCA II (PDB ID: 4BF1, resolution 1.35 Å)[40], hCA IX (PDB code: 4Z0Q, resolution 1.45 Å)[41] and hCA XII (PDB code: 1JD0, resolution 1.50 Å)[42] were obtained from the Protein Data Bank (www.pdb.org). The downloaded crystal structure was prepared using the Schrodinger 2021 suite package's preparation wizard with the default settings and pH value of 7.4. ChemDraw Professional 17.0 was employed to sketch the ligands, which were then exported in the structure data file format (SDF) and sent to the Ligprep module. The Schrodinger Ligprep module was then utilised in the ligand preparation process to further optimise the geometry. Glide's extra precision module was used to dock the minimised ligands inside the binding cavity of the appropriate crystal structure, generating 10 poses per docked ligand. The pose with the most negative docking score was chosen to display.

3. Results and discussion

3.1. Chemical synthesis

Scheme 1 depicts the synthetic route utilised to produce the target compounds **4a–l**. Refluxing of 2-amino-5-bromobenzonitrile (**1a**) or 2-amino-4-bromobenzonitrile (**1b**) with N,N-dimethylformamide dimethyl acetal (DMF-DMA) yielded intermediates **2a–b**. Compounds **3a–d** were synthesised by reacting the appropriate sulphonamide with the intermediates **2a–b** in glacial acetic acid (GAA) under reflux. Using Suzuki reaction compounds **3a–d** were subsequently reacted with the suitable boronic acid derivative employing the coupling catalyst Pd(amphos)C12 and the inorganic base T3P (propylphosphonic anhydride) dissolved in dioxane and water at 80 °C under pressure in the presence of nitrogen to produce compounds **4a–l**. The chemical structures and purity of the synthesised target compounds were determined using NMR, HRMS, and HPLC analytical techniques[43–45]. The ^{1}H NMR spectra of compounds **3a–d** exhibited a characteristic peak at the range of 7.20–7.50 ppm which can be attributed to the sulphonamide NH_2 and a second peak at 10.10–10.30 ppm attributable to the NH of the amide group verifying the successful synthesis of the
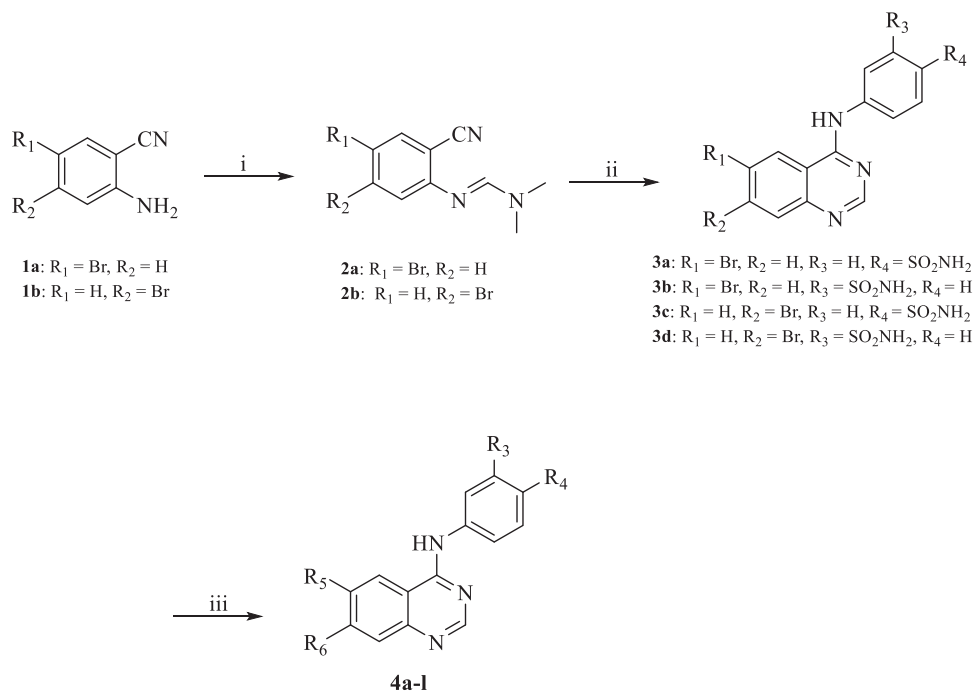
Scheme 1. Reagents and conditions: (i) DMF-DMA, 100 °C, 1.5 h; (ii) appropriate aniline, GAA, reflux, 2 h; (iii) suitable boronic acid derivative, Pd(amphos)C12, T3P, dioxane, 80 °C, 2 h (For **4a–l**, R_5 and R_6 are described in detail in Table 1).

intermediates **3a–d** from their parent compounds **2a–b**. Suzuki cross-coupling reactions success was verified by the presence of the appropriate characteristic peaks in the ^{1}H NMR spectra of compounds **4a–l**. For example, compound **4b** ^{1}H NMR spectra was characterised by the appearance of a new singlet peak at 10.20 ppm attributable to the carbonyl moiety. Similarly, compound **4i** was characterised by the appearance of new singlet peak at 10.38 ppm due to the carbonyl group of the tetrahydro-furan-2-carbaldehyde moiety. In a similar manner, the synthesis of compounds **4j** and **4k** was confirmed by the appearance of a singlet peak at 10.10 and 10.14 ppm, respectively, attributable to the hydroxy group of the phenol moiety. Compound **4e** synthesis was confirmed by the presence of a singlet peak at 3.82 ppm attributable to the three hydrogens of the methoxy group. Likewise, the appearance of two multiple peaks in the aliphatic region of the ^{1}H NMR spectrum of compound **4h** attributable to the eight hydrogens of the morpholine ring confirmed its successful synthesis.

3.2. Carbonic anhydrase inhibition study

As indicated in Table 1, the biological evaluation of CA inhibitory activities of compounds **3a–b**, **4a–l** and AAZ as a standard inhibitor, was performed on a panel of four hCA isoforms by a stopped flow CO_2 hydrase assay. This panel comprised the two ubiquitously expressed cytosolic hCA I and II isoforms, along with the two tumour-related transmembrane hCA IX and XII isoforms. With respect to the first cytosolic isoform (hCA I) the structural hybrid compounds **3a**, **4e**, **4f** showed greater inhibitory activities when compared with the standard AAZ, which possessed an inhibition constant (K_i) of 250.0 nM, exhibiting inhibitory activity of 89.4, 91.2 and 60.9 nM, respectively. In all three compounds the substitution at the 6- position of the aromatic quinazoline ring was occupied by a hydrophobic substituent and the sulphonamide moiety was in the para position. Interestingly, compound **3a** analogue, Compound **3b,** with a meta-substituted sulphonamide, lost all activity against the first cytosolic isoform hCA I. Similarly, other quinazolines with a hydrophilic "tail" or a meta-substituted sulphonamides lost all inhibitory activity against hCA I. As such the SAR of the synthesised hybrids against the first cytosolic isoform (hCA I) can be summarised in Figure 5(A).

Similarly, compounds **3a**, **4e** and **4f** showed potent inhibition for the physiologically dominant isoform hCA II with inhibitory concentrations of 8.7, 4.6 and 37.1 nM, respectively. Furthermore, compounds **4a**, **4c** and **4j** exhibited inhibitory potent activities of 2.4, 47.1 and 66.3 nM, respectively. These results indicate that the positioning of the sulphonamide group is essential for determining the activity, with para-substituted sulphonamides being essential for activity. This conclusion was further verified by the loss of

activity of compounds **3b**, **4k** and **4l** when compared to their respective potent analogues **3a**, **4a** and **4j**, respectively. Conversely, the nature of the aromatic substitution at positions 6 and 7 of the quinazoline ring, did not affect activity, with both hydrophilic and hydrophobic substitutions showing promising activity against hCA II isoform. However, the smaller substituents exhibited higher potency when compared to larger ones. The predicted SAR for the synthesised hybrids against hCA II isoform is illustrated in Figure 5(B).

All synthesised hybrid compounds demonstrated significant inhibitory activity for the tumour associated isoforms hCA IX and XII. Among the synthesised compounds, **4f** exhibited the highest potency against hCA IX (K_i of 86.5 nM), while compound **3b** was the most potent of the synthesised hybrids against hCA XII, with an inhibitory concentration of 39.4 nM.

3.3. Molecular docking study

In computer-aided drug design research, the prediction of binding modes of a ligand and its proposed target, in addition to the correlation of the obtained scores with prospective activity, are all useful applications of molecular docking[46]. Another benefit of molecular docking studies is the ability to predict the effect of specific amino acid mutations on the activity profile of the ligand[47]. Furthermore, visualising the docking study's consequent interactions assists future ligand modification, leading to compounds possessing improved binding characteristics[48]. Hence, the synthesised hybrids were subjected to a molecular docking study against hCA I, II, IX and XII isozymes to correlate the structural characteristic features with the reported inhibitory activity and examine the binding profile of the synthesised hybrids. Generally, the co-crystalized ligands in hCA isoforms I and II and IX exhibited the typical sulphonamide moiety pattern, where the sulphonamide moiety binds to the zinc(II) ion following the displacement of the metal-bound water molecule to establish the tetrahedral adduct with the zinc atom[49].

Out of the synthesised hybrids the compounds exhibiting the highest activity, compounds **4a** and **4f,** were subjected to a molecular docking study. Among the synthesised hybrids, compound **4f** exhibited the highest potency against both the hCA I and IX isoforms with inhibitory activity of 60.9 nM and 86.5 nM, respectively. Compound **4f** (60.9 nM), adhered to the general pattern of the benzenesulfonamide ring fitting deeply within the shallow CA active site through the anchoring the zinc atom in a characteristic manner for sulphonamide CAIs through an NH$^-$ and Zn^{2+} bond. In addition to the typical zinc metal-ligand interactions compound **4f** formed a hydrogen bond between the carbonyl moiety of the sulphonamide moiety and THR199 of the active site (Figure 6(B)). Compound **4f** exhibited another hydrogen
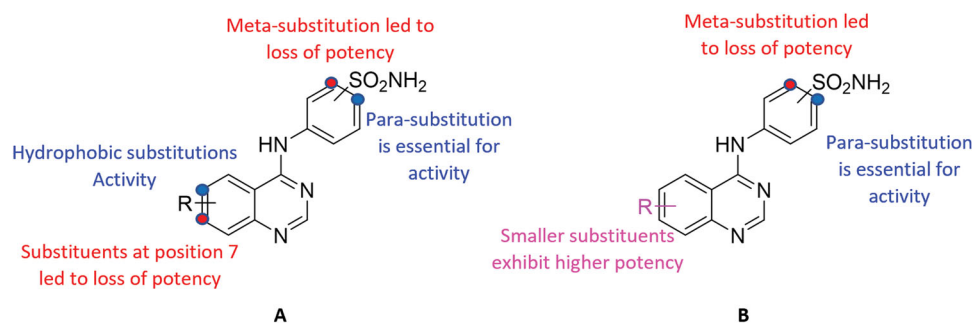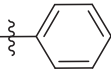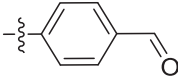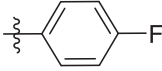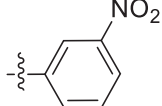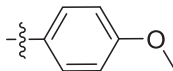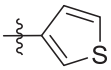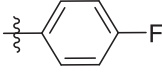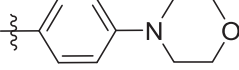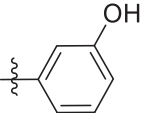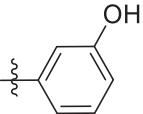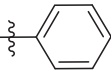

Figure 5. The predicted SAR of the synthesised hybrids against hCA I (A) and hCA II (B) isoforms.

bond between the amide moiety (NH) and PRO201 amino acid residues. Moreover, compound **4f** established two $\pi-\pi$ interactions with PHE91 and HIS200 amino acid residues, further increasing the compound's affinity to the active site. Compound **4f** was equally potent against hCA IX, which was due to the formation of two metal interactions between the sulphonamide group and the zinc atom of the active site. Furthermore, compound **4f** established a hydrogen bond with THR199 and weak hydrophobic

Table 1. The inhibitory activity (K_i) of the synthesised hybrids against hCA I, II, IX and XII isoforms

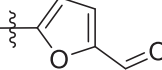| Cpd	R_3	R_4	R_5	R_6	K_i (nM) hCA I	hCA II	hCA IX	hCA XII
3a	H	SO_2NH_2	Br	H	89.4	8.7	174.0	46.5
3b	SO_2NH_2	H	Br	H	7102	5758	95.3	39.4
4a	H	SO_2NH_2	(phenyl)	H	600.0	2.4	180.3	65.7
4b	H	SO_2NH_2	(4-formylphenyl)	H	650.7	303.8	86.9	67.4
4c	H	SO_2NH_2	(4-fluorophenyl)	H	931.4	47.1	559.6	93.0
4d	H	SO_2NH_2	(3-nitrophenyl)	H	588.2	55.7	265.3	90.7
4e	H	SO_2NH_2	(4-methoxyphenyl)	H	91.2	4.6	86.9	77.0
4f	H	SO_2NH_2	(thiophen-3-yl)	H	60.9	37.1	86.5	89.5
4g	SO_2NH_2	H	(4-fluorophenyl)	H	3125	231.0	229.0	30.5
4h	H	SO_2NH_2	(4-morpholinophenyl)	H	548.4	112.3	336.8	49.8
4i	SO_2NH_2	H	(5-formylfuran-2-yl)	H	5583	2419	487.9	52.7
4j	H	SO_2NH_2	H	(3-hydroxyphenyl)	361.3	66.3	244.8	66.7
4k	SO_2NH_2	H	H	(3-hydroxyphenyl)	4680	2525	90.3	69.7
4l	SO_2NH_2	SO_2NH_2	(phenyl)	H	6565	678.3	88.8	89.4
AAZ	–	–	–	–	250.0	12.1	25.7	5.7

Figure 6. The binding patterns of compound **4f** inside the binding cavity of hCAI and IX. (A) 3D model of the crystal structure of hCA I with compound **4f**. (B) 2D interaction pattern of compound **4f** with hCA I binding cavity. (C) 3D model of the crystal structure of hCA IX with compound **4f**. (D) 2D interaction pattern of compound **4f** with hCA IX binding cavity.

Figure 7. The 2D interaction patterns of compound **4f** with hCA II (A) and XII (B). Favourable interactions are colour coded as follows: purple–hydrogen bond, grey–metal bond, red–π-cation interaction, green–π–π stacking interactions. The light green lines represent weak van der Waals interactions.

interactions with the amino acid residues of the active site (Figure 6(D)).

The docking of compound **4f** against hCA II and XII isoforms revealed a similar interaction pattern, with the sulphonamide moiety fitted deeply inside the binding site groove. Furthermore, compound **4f** established a hydrogen bond interaction with THR199 amino acid residue of hCA II and XII active sites (Figure 7), indicating that the formation of a hydrogen bond with THR199

is essential for the activity of carbonic anhydrase inhibitors. The potent inhibitory activity of compound **4f** ($K_i = 89.5$ nM) can be further explained through the compound's ability to establish an additional π-cation bond with LYS67 as well as a π–π stacking interaction with HIS94 (Figure 7(B)). The 2D interaction pattern of compound **4f** with hCA II and XII is illuminated in Figure 7, while the corresponding 3D models are demonstrated in the Supplementary file (Figure S4.1–2).
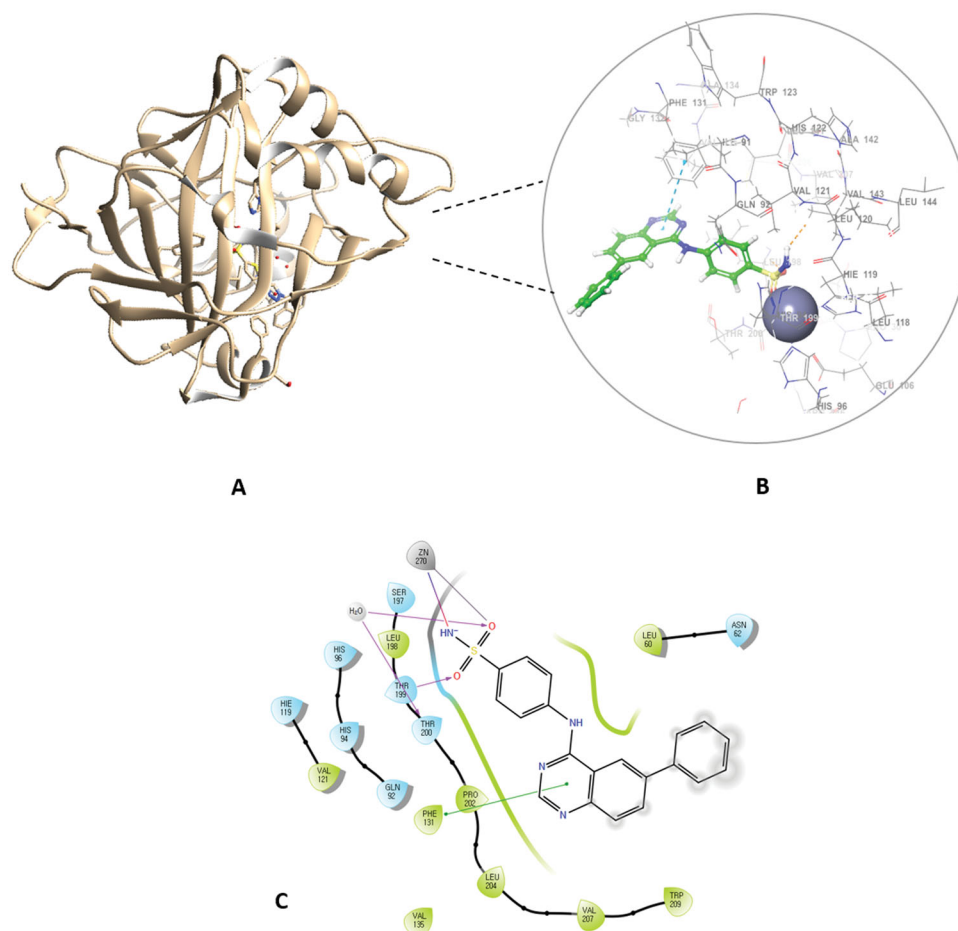
Figure 8. The docked complex of compound **4a** with hCA II isoform. (A) 3D model of the crystal structure of hCA II with compound **4a**, (B) 3D docking pose of compound **4a**, favourable interactions are exhibited as dashed lines: orange–hydrogen bonds, blue–π-π stacking, (C) 2D interaction pattern of compound **4a** with hCA II binding cavity, favourable interactions are colour coded as follows: green–π-π stacking, purple–hydrogen bonds, grey–metal interactions and light green–weak van der Waals interactions.

Comparably, compound **4a,** which possessed the highest potency against the hCA II isoform ($K_i = 2.4$ nM) when docked in the active site hCA II, formed the typical metal interaction of the sulphonamide group with the Zn metal as well as a hydrogen bond with THR199 and π-π stacking interaction between the quinazoline ring and PHE131 (Figure 8). The interaction of compound **4a** against the remaining isoforms is illustrated in the Supplementary file.

4. Conclusion

Herein, the design, synthesis, and characterisation of a novel series of quinazoline-based sulphonamides were reported and their activities against hCA I, II, IX and XII isoforms were assessed. Most of the newly synthesised quinazoline sulphonamide hybrids efficiently inhibited the investigated hCA I, II, IX and XII, with inhibitory activity in the single digit nanomolar range. Among the synthesised compounds, compound **4f** possessed the highest potency against hCA I and IX isoforms with a K_i of 60.9 nM and 86.5 nM, respectively. Against the hCA II isoform, compound **4a** displayed the highest inhibitory activity of 2.4 nM. Compound **4g** was the most potent inhibitor against hCA XII with K_i of 30.5 nM. Additionally, compounds **3a** and **4b** possessed single digit inhibitory activity against hCA II of 8.7 and 4.6 nM, respectively. Compounds **3a** and **4e** were able to inhibit hCA I at concentrations of 89.4 and 91.2 nM, which is more potent when compared

to the inhibitory concentration of the standard Acetazolamide (250 nM). Furthermore, all tested compounds displayed potent activity against the hCA XII isoform, with inhibitory activities ranging from 30.5–93 nM. The SAR of the synthesised hybrids were predicted based on the obtained biological data. Finally, a molecular docking study was conducted to provide insights on the binding interactions of the most potent compound for each tested hCA isoform.

Disclosure statement

CT Supuran is Editor-in-Chief of the Journal of Enzyme Inhibition and Medicinal Chemistry. He was not involved in the assessment, peer review, or decision-making process of this paper. The authors have no relevant affiliations of financial involvement with any organisation or entity with a financial interest in or financial

conflict with the subject matter or materials discussed in the manuscript. This includes employment, consultancies, honoraria, stock ownership or options, expert testimony, grants or patents received or pending, or royalties.

Funding

ORCID

Hossam Nada http://orcid.org/0000-0002-4882-5621
Ahmed Elkamhawy http://orcid.org/0000-0001-7398-6155
Magda H. Abdellattif http://orcid.org/0000-0002-8562-4749
Andrea Angeli http://orcid.org/0000-0002-1470-7192
Claudiu T. Supuran http://orcid.org/0000-0003-4262-0323

References

1. Supuran CT, Scozzafava A. Carbonic anhydrases as targets for medicinal chemistry. Bioorg Med Chem 2007;15:4336–50.
2. Supuran CT. Carbonic anhydrases: novel therapeutic applications for inhibitors and activators. Nat Rev Drug Discov 2008;7:168–81.
3. Topal F, Aksu K, Gulcin I, et al. Inhibition profiles of some symmetric sulfamides derived from phenethylamines on human carbonic anhydrase I, and II isoenzymes. Chem Biodivers 2021;18:e2100422.
4. Durdagi S, Şentürk M, Ekinci D, et al. Kinetic and docking studies of phenol-based inhibitors of carbonic anhydrase isoforms I, II, IX and XII evidence a new binding mode within the enzyme active site. Bioorg Med Chem 2011;19: 1381–9.
5. Nocentini A, Donald WA, Supuran CT. Chapter 8 – human carbonic anhydrases: tissue distribution, physiological role, and druggability. In: Supuran CT, Nocentini A, eds. Carbonic anhydrases. Cambridge: Academic Press; 2019:151–185.
6. Quade BN, Parker MD, Occhipinti R. The therapeutic importance of acid-base balance. Biochem Pharmacol 2021;183: 114278.
7. Supuran CT, Scozzafava A. Carbonic anhydrase inhibitors and their therapeutic potential. Expert Opin Ther Pat 2000; 10:575–600.
8. Mohamed MM, Sloane BF. Cysteine cathepsins: multifunctional enzymes in cancer. Nat Rev Cancer 2006;6:764–75.
9. Annan DA, Maishi N, Soga T, et al. Carbonic anhydrase 2 (CAII) supports tumor blood endothelial cell survival under lactic acidosis in the tumor microenvironment. Cell Commun Signal 2019;17:169
10. Cuffaro D, Nuti E, Rossello A. An overview of carbohydrate-based carbonic anhydrase inhibitors. J Enzyme Inhib Med Chem 2020;35:1906–22.
11. Awadallah FM, Bua S, Mahmoud WR, et al. Inhibition studies on a panel of human carbonic anhydrases with N1-substituted secondary sulfonamides incorporating thiazolinone or imidazolone-indole tails. J Enzyme Inhib Med Chem 2018;33: 629–38.
12. Supuran CT. Experimental carbonic anhydrase inhibitors for the treatment of hypoxic tumors. J Exp Pharmacol 2020;12: 603–17.
13. Sanku RKk. Development and biological evaluation of carbonic anhydrase modulators as potential nootropics and anticancer agents. Ann Arbor: Temple University; 2018, pp. 154.
14. Supuran CT. Advances in structure-based drug discovery of carbonic anhydrase inhibitors. Expert Opin Drug Discov 2017;12:61–88.
15. Supuran CT. Exploring the multiple binding modes of inhibitors to carbonic anhydrases for novel drug discovery. Expert Opin Drug Discov 2020;15:671–86.
16. Aggarwal M, Kondeti B, McKenna R. Insights towards sulfonamide drug specificity in α-carbonic anhydrases. Bioorg Med Chem 2013;21:1526–33.
17. Carta F, Supuran CT, Scozzafava A. Sulfonamides and their isosters as carbonic anhydrase inhibitors. Future Med Chem 2014;6:1149–65.
18. McDonald PC, Chia S, Bedard PL, et al. A phase 1 study of SLC-0111, a novel inhibitor of carbonic anhydrase IX, in patients with advanced solid tumors. Am J Clin Oncol 2020; 43:484–90.
19. Hampson AJ, Babalonis S, Lofwall MR, et al. A pharmacokinetic study examining acetazolamide as a novel adherence marker for clinical trials. J Clin Psychopharmacol 2016;36: 324–32.
20. Yuan L, Wang M, Liu T, et al. Carbonic anhydrase 1-mediated calcification is associated with atherosclerosis, and methazolamide alleviates its pathogenesis. Front Pharmacol, 2019;10:766.
21. Yu-Jing YJ, Zhang CM, Liu ZP. Recent developments of small molecule EGFR inhibitors based on the quinazoline core scaffolds. Anticancer Agents Med Chem 2012;12:391–406.
22. Elkamhawy A, Farag AK, Viswanath AN, et al. Targeting EGFR/HER2 tyrosine kinases with a new potent series of 6-substituted 4-anilinoquinazoline hybrids: design, synthesis, kinase assay, cell-based assay, and molecular docking. Bioorg Med Chem Lett 2015;25:5147–54.
23. Cohen MH, Williams GA, Sridhara R, et al. FDA drug approval summary: gefitinib (ZD1839) (Iressa) tablets. The Oncologist 2003;8:303–6.
24. Johnson JR, Cohen M, Sridhara R, et al. Approval summary for erlotinib for treatment of patients with locally advanced or metastatic non-small cell lung cancer after failure of at least one prior chemotherapy regimen. Clin Cancer Res 2005;11:6414–21.
25. Cortazar P, Justice R, Johnson J, et al. US Food and Drug Administration approval overview in metastatic breast cancer. J Clin Oncol 2012;30:1705–11.
26. Zhang D, Pal A, Bornmann WG, et al. Activity of lapatinib is independent of EGFR expression level in HER2-overexpressing breast cancer cells. Mol Cancer Ther 2008;7:1846–50.
27. Degrauwe N, Sosa JA, Roman S, Deshpande HA. Vandetanib for the treatment of metastatic medullary thyroid cancer. Clin Med Insights Oncol 2012;6:CMO.S7999.
28. Tan F, Shi Y, Wang Y, et al. Icotinib, a selective EGF receptor tyrosine kinase inhibitor, for the treatment of non-small-cell lung cancer. Future Oncol 2015;11:385–97.
29. Yu HA, Pao W. Targeted therapies: Afatinib-new therapy option for EGFR-mutant lung cancer. Nature Rev Clin Oncol 2013;10:551–2.

30. Asif M. Chemical characteristics, synthetic methods, and biological potential of quinazoline and quinazolinone derivatives. Int J Med Chem 2014;2014:395637.

31. Elkamhawy A, Viswanath AN, Pae AN, et al. Discovery of potent and selective cytotoxic activity of new quinazoline-ureas against TMZ-resistant glioblastoma multiforme (GBM). Eur J Med Chem 2015;103:210–22.

32. Alafeefy AM, Ceruso M, Al-Tamimi A-MS, et al. Quinazoline-sulfonamides with potent inhibitory activity against the α-carbonic anhydrase from Vibrio cholerae. Bioorg Med Chem 2014;22:5133–40.

33. Alafeefy AM, Ceruso M, Al-Jaber NA, et al. A new class of quinazoline-sulfonamides acting as efficient inhibitors against the α-carbonic anhydrase from Trypanosoma cruzi. J Enzyme Inhib Med Chem 2015;30:581–5.

34. Lee K, Nada H, Byun HJ, et al. Hit identification of a Novel quinazoline sulfonamide as a promising EphB3 inhibitor: design, virtual combinatorial library, synthesis, biological evaluation, and docking simulation studies. Pharmaceuticals. 2021;14:1247.

35. Maresca A, Temperini C, Vu H, et al. Non-zinc mediated inhibition of carbonic anhydrases: coumarins are a new class of suicide inhibitors. J Am Chem Soc 2009;131:3057–62.

36. Menchise V, De Simone G, Alterio V, et al. Carbonic anhydrase inhibitors: stacking with Phe131 determines active site binding region of inhibitors as exemplified by the X-ray crystal structure of a membrane-impermeant antitumor sulfonamide complexed with isozyme II. J Med Chem 2005;48:5721–7.

37. Margheri F, Ceruso M, Carta F, et al. Overexpression of the transmembrane carbonic anhydrase isoforms IX and XII in the inflamed synovium. J Enzyme Inhib Med Chem 2016;31:60–3.

38. Bozdag M, Ferraroni M, Nuti E, et al. Combining the tail and the ring approaches for obtaining potent and isoform-selective carbonic anhydrase inhibitors: solution and X-ray crystallographic studies. Bioorg Med Chem 2014;22:334–40.

39. Ali M, Bozdag M, Farooq U, et al. Benzylaminoethyureido-tailed benzenesulfonamides: design, synthesis, kinetic and X-ray investigations on human carbonic anhydrases. Int J Mol Sci. 2020;21:2560.

40. Leitans J, Sprudza A, Tanc M, et al. 5-Substituted-(1,2,3-triazol-4-yl)thiophene-2-sulfonamides strongly inhibit human carbonic anhydrases I, II, IX and XII: solution and X-ray crystallographic studies. Bioorg Med Chem 2013;21:5130–8.

41. Buemi MR, De Luca L, Ferro S, et al. Carbonic anhydrase inhibitors: design, synthesis and structural characterization of new heteroaryl-N-carbonylbenzenesulfonamides targeting druggable human carbonic anhydrase isoforms. Eur J Med Chem 2015;102:223–32.

42. Whittington DA, Waheed A, Ulmasov B, et al. Crystal structure of the dimeric extracellular domain of human carbonic anhydrase XII, a bitopic membrane protein overexpressed in certain cancer tumor cells. Proc Natl Acad Sci USA. 2001;98:9545–50.

43. Elkamhawy A, Kim NY, Hassan AHE, et al. Design, synthesis and biological evaluation of novel thiazolidinedione derivatives as irreversible allosteric IKK-β modulators. Eur J Med Chem 2018;157:691–704.

44. Park JE, Elkamhawy A, Hassan AHE, et al. Synthesis and evaluation of new pyridyl/pyrazinyl thiourea derivatives: neuroprotection against amyloid-β-induced toxicity. Eur J Med Chem 2017;141:322–34.

45. Al-Sanea MM, Elkamhawy A, Zakaria A, et al. Synthesis and in vitro screening of phenylbipyridinylpyrazole derivatives as potential antiproliferative agents. Molecules 2015;20:1031–45.

46. Macalino SJY, Gosu V, Hong S, Choi S. Role of computer-aided drug design in modern drug discovery. Arch Pharm Res 2015;38:1686–701.

47. Guedes IA, de Magalhães CS, Dardenne LEJBr. Receptor-ligand molecular docking. Biophys Rev. 2014;6:75–87.

48. Wang J, Li Y, Yang Y, et al. In silico research to assist the investigation of carboxamide derivatives as potent TRPV1 antagonists. Mol BioSystems 2015;11:2885–99.

49. Shaldam M, Nocentini A, Elsayed ZM, et al. Development of novel Quinoline-based sulfonamides as selective cancer-associated carbonic anhydrase isoform IX inhibitors. Int J Mol Sci 2021;22:11119.